iScience

CellPress
OPEN ACCESS

Article

A collision-free gallop-based triboelectric-piezoelectric hybrid nanogenerator

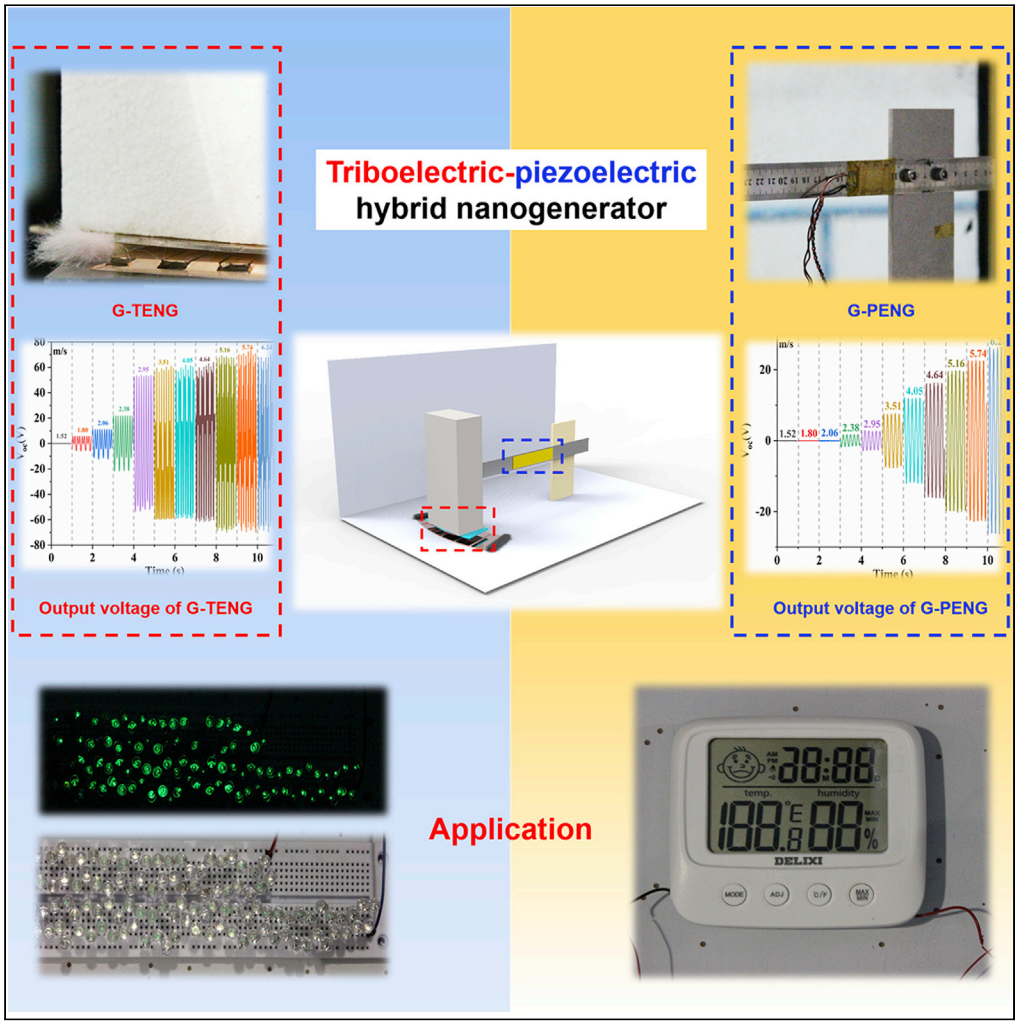

Weizhe Wang, Wei Tang, Zhaohui Yao

tangwei@binn.cas.cn (W.T.)
yaozh@ucas.edu.cn (Z.Y.)

Highlights

A gallop-based triboelectric-piezoelectric hybrid nanogenerator is proposed

Piezoelectric sheets are attached to beam to improve the performance of HG P-TENG

A segmenting electrodes method is used to improve the energy harvesting efficiency

Rabbit fur can effectively reduce material wear and improve system durability

Wang et al., iScience 25, 105374
November 18, 2022
https://doi.org/10.1016/j.isci.2022.105374

iScience

CellPress
OPEN ACCESS

Article

A collision-free gallop-based triboelectric-piezoelectric hybrid nanogenerator

Weizhe Wang,[1] Wei Tang,[2,3,*] and Zhaohui Yao[1,4,*]

SUMMARY

Energy harvesting technologies that convert fluid energy into usable electrical energy are of great significance, especially in long-distance pipeline systems. Here, in order to avoid the collision of conventional galloping triboelectric nanogenerators (GTENGs), and cause material damage or noise, a freestanding gallop-based triboelectric-piezoelectric hybrid nanogenerator (HG P-TENG) is proposed to reduce material wear and improve the reliability of GTENG. Two piezoelectric sheets are attached to the cantilever beam. The root-mean-square (RMS) and peak output power of the HG P-TENG are 68.9 μW and 1.27 mW, respectively. To improve the harvesting efficiency, the fixed copper electrodes are segmented, and experiments indicate that this way of segmenting electrodes can improve the energy harvesting efficiency. Finer electrodes can effectively increase the charging rate of capacitors. A self-powered thermohygrometer and light-emitting diodes (LEDs) are demonstrated in the wind tunnel. It demonstrates that the proposed hybrid nanogenerator will exhibit great potential in pipeline systems.

INTRODUCTION

With the development of the Internet of Things and the digital Internet, a large number of distributed micro-sensors are required to collect various information. These sensors require low power, some as little as a few microwatts, but still need to be powered by conventional methods such as batteries. Traditional batteries have the disadvantages of large size, environmental pollution, and need to be replaced periodically (Beeby et al., 2006), whereas obtaining energy from the environment through an energy harvester can effectively provide a durable and stable energy supply for the micro-sensor. There are various types of energy in the environment, such as solar energy, wind energy, tidal energy, biomass energy, etc., and wind energy is undoubtedly an inexhaustible and very clean energy. So far, energy harvesting technologies have been extensively developed in several types: triboelectric (Liu et al., 2021; Chen et al., 2018; Fan et al., 2012; Wang et al., 2017; Wang, 2014), piezoelectric (Abdelkefi et al., 2014; Alhadidi et al., 2020; Wang et al., 2021; Hu et al., 2018a), electrostatic (Mitcheson et al., 2004; Basset et al., 2014), pyroelectric (He et al., 2022b), and electromagnetic (Avila Bernal and Linares García, 2012; He et al., 2022a; Vicente-Ludlam et al., 2014). Compared to several other energy harvesting techniques, the use of piezoelectric and triboelectric is more suitable for this type of low frequency vibration, and a more systematical comparison is shown in Table S1. Therefore, providing stable energy for micro-sensors via triboelectric nanogenerator (TENG) and piezoelectric nanogenerator (PENG) is a feasible solution.

Since TENG was proposed by Wang (Fan et al., 2012) in 2012, a lot of research work has been done on TENG and it has been widely used in various scenarios, such as wearable electronic devices (Wang et al., 2013; Tee et al., 2012; Xu et al., 2021), micro-sensors (Li et al., 2021; Yang et al., 2021) and energy harvesting (Park et al., 2019; Zhang et al., 2021b; Wang et al., 2015, 2021), and other related work. Long-distance pipeline contains enormous amounts of energy, so energy harvesting is a feasible way to power pipeline monitoring devices. TENG for gas energy harvesting is a very interesting area of research. There are three main types: fluttering (Hu et al., 2019; Ren et al., 2021; Olsen et al., 2019; Bae et al., 2014; Wang et al., 2020d; Jiang et al., 2020), rotary (Wen et al., 2015; Li et al., 2022; Fu et al., 2021), and galloping (Zhang et al., 2020a; Wang et al., 2020c). Xia et al. investigated the effects of wind speed, length and thickness of the film, and spacing between the upper and lower of two flat electrodes on the performance of the TENG. The results show that choosing appropriate structural parameters can effectively improve the performance of the energy harvester and reduce the cut-in wind speed (Xia et al., 2021). Lin et al. designed an

[1]School of Engineering Science, University of Chinese Academy of Sciences, Beijing 101408, China

[2]Beijing Institute of Nanoenergy and Nanosystems, Chinese Academy of Sciences, Beijing 100083, China

[3]School of Nanoscience and Technology, University of Chinese Academy of Sciences, Beijing 100049, China

[4]Lead contact

*Correspondence: tangwei@binn.cas.cn (W.T.), yaozh@ucas.edu.cn (Z.Y.)

https://doi.org/10.1016/j.isci.2022.105374

angle-shaped TENG (AS-TENG) that effectively increased the contact area between fluorinated ethylene-propylene (FEP) film and aluminum electrode. The AS-TENG can be facilely integrated into a 360° radial array, which greatly increased the effective area of the whole system with high level of integration. At the same time, a wedge-shaped wind guide channel is also proposed to reduce the cut-in wind speed, which is more suitable for collecting breezes (Lin et al., 2019). In addition, more and more researchers are using rotary sliding triboelectric nanogenerators (RS-TENGs) to harvest wind energy. Xie et al. first proposed a rotary cup-structured triboelectric nanogenerator (R-TENG) to drive the flexible polytetrafluoroethylene (PTFE) to continuously sweep across an aluminum sheet under the action of breezes in the environment, and the energy was collected through continuous contact separation (Xie et al., 2013). Zhang et al. studied elastic rotary triboelectric nanogenerators (ER-TENGs), which effectively reduced the friction between electrodes through material selection and structural design. Compared with conventional ER-TENGs, the energy harvesting efficiency is doubled and the durability is even quadrupled, greatly improving the practicality of the device (Zhang et al., 2021a). Most of the current research is still focused on the exploitation of R-TENG for wind energy harvesting. However, using galloping for energy harvesting has the advantage of a simpler structure and high robustness (Hu et al., 2018b). Therefore, a gallop-based TENG is designed. Zhang et al. created a galloping triboelectric nanogenerator (GTENG) based on contact electrification between two flexible beams. It is able to achieve an output voltage of more than 200 V at a low wind speed of 1.4 m/s through the cross-flow galloping vibration of a main beam with a prism and collision with an auxiliary beam (Zhang et al., 2020a). Zeng has developed a novel TENG based on the flow-induced vibration (FIV) effect (FIV-TENG) which is packed into a bluff body. It not only reduces the environmental interference, but also avoids the huge rotational resistance and frictional wear faced by ordinary TENGs (Zeng et al., 2020; Ren et al., 2020). However, this type of beating can easily cause permanent damage to the structure. The reliability of the GTENG is one of the most important considerations, while durability and robustness are also key issues (Li et al., 2020). It is necessary to develop a structure that can work for a long time without damaging the material.

To solve the problems of low reliability and poor durability of current GTENG, in this paper, a gallop-based triboelectric-piezoelectric hybrid nanogenerator (HG P-TENG) is proposed. In order to reduce system damping, most areas of the structure are designed to be non-contact, which also can reduce the cut-in wind speed and at the same time reduce the friction loss of material. Although the charges on the surface of FEP material can be stored for several days, it will dissipate gradually and is not suitable for long-time operation. Therefore, the flexible rabbit fur brushes are designed on the outer side of the both sides of electrode for periodic contact with the FEP film to continuously provide charges to the FEP surface. Furthermore, the electrode layers are segmented and the results show that the 6-degrees G-TENG has higher performance which can generate an RMS and peak power of 52.2 μW and 1.13 mW at a wind speed of 6.24 m/s. Although the 2-degrees G-TENG has only an RMS power of 34.7 μW, it can generate more current cycles in one period, thereby charging the capacitor faster. At the same time, to increase the power output, two piezoelectric sheets are attached to the cantilever beam, and the maximum output power of the piezoelectric sheets is about 16.7 μW when the wind speed is 6.24 m/s. To demonstrate the durability of the HG P-TENG, about 250,000 cycles were tested with only a slight decrease in voltage. This fully illustrates the advantages of hybrid nanogenerator in terms of improving power and durability of energy harvesting. To reveal its great potential in smart pipeline monitoring systems, the feasibility of this HG P-TENG to power thermohygrometer and light-emitting diodes (LEDs) at a wind speed of 6.24 m/s is also investigated.

RESULTS AND DISCUSSION

Structure design and principle

The whole experiment is carried out in a circulating wind tunnel, which can generate a highly uniform incoming flow with a turbulence degree of about 0.5%, and the cross-sectional size of the experimental section is 50 × 50 cm Figure 1E shows the photograph of HG P-TENG, including G-PENG (Galloping PENG) and G-TENG (Galloping TENG). The structure of HG P-TENG is mainly divided into two parts, the first part is the wind vibration transducer, which uses the galloping vibration for energy harvesting. The cantilever beam is mounted on a bracket, and a foam prism is mounted on top of the cantilever beam. Galloping occurs when the wind flows through the prism (Vedio S1). At the bottom of the prism, there is a curved acrylic plate with an angle of 26°, and the FEP film is adhered to acrylic plate (Figure S1). The second part is a fixed free-standing layer with curved copper electrodes mounted on the acrylic directly below the film. Since the motion of this prism is a circular motion with the length of the cantilever beam as the radius, the electrode

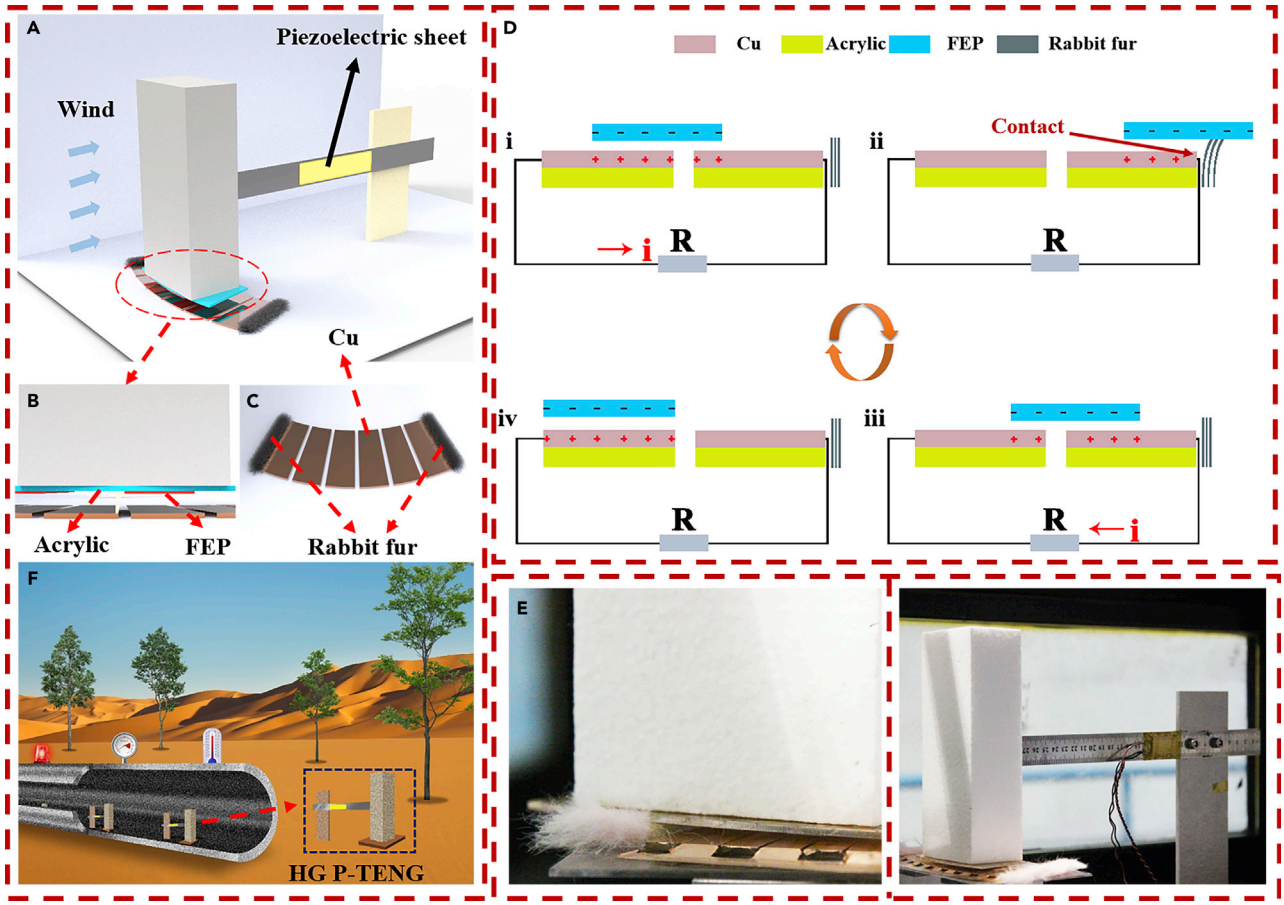

Figure 1. Structure diagram of triboelectric-piezoelectric hybrid nanogenerator (HG P-TENG)

(A) Overall schematic of HG P-TENG.

(B) Schematic diagram of dielectric layer.

(C) Schematic diagram of 6-degrees of Cu electrodes layer.

(D) Schematic diagram for the working principle of G-TENG.

(E) Photograph of the FEP dielectric layer and hybrid nanogenerator.

(F) Application scenario of HG P-TENG in pipeline.

layer is also designed to be circular to always remain parallel to the FEP, as shown in Figure 1A. In order to make the FEP film always move on the copper electrode, the radius of the copper electrode should be slightly larger than that of the FEP film, which can effectively prevent the energy loss caused by the incomplete overlapping of the electrodes due to the installation deviation during the movement of the FEP film. A typical application scenario is shown in Figure 1F.

The working principle of HG P-TENG is shown in Figure 1, which mainly consists of two parts. The first part is the piezoelectric nanogenerator. It consists of two pieces polyvinylidene fluoride for energy harvesting using the piezoelectric effect (Figure S2). Two piezoelectric sheets connected in parallel on two sides of the cantilever beam are bent under the influence of the galloping of the prism, resulting in positive and negative charges on its upper and lower surfaces. The second part is the triboelectric nanogenerator. In Figure 1DI, the prism vibration moves from left to right, and will form a left-to-right current in the external circuit. The prism continues to move to the right, and the FEP dielectric layer under the prism will contact the rabbit fur brushes in Figure 1D(ii). The rabbit fur is not only an excellent electropositive material but also has low frictional resistance. According to the list of triboelectric series, the difference in triboelectric series between FEP and rabbit fur is so large. Therefore, when the two are in contact, electrons on the surface of rabbit fur will be transferred to the FEP, which makes the FEP surface negatively charged and the rabbit hair positively charged (Chen et al., 2021; Davies, 1969; McCarty and Whitesides, 2008; Zhu et al., 2012). And the

surface charges will be saturated after several such cycles. Due to the high stiffness of the cantilever beam, when the cantilever beam reaches the limit of bending to the right in Figure 1D(ii), the velocity will decrease to zero and start to accelerate to the left. When the FEP dielectric layer moves from the right side to the left side, a reverse current will be generated in Figure 1D(iii). The prism will continue to move until it reaches the limit on the left and will move to the right in Figure 1D(iv). So, when the wind passes through the prism, the HG P-TENG will constantly harvest wind energy.

Galloping vibration analysis

The paper uses galloping method for energy harvesting, which reduces the complexity of the structure and improves the robustness. There are four vibration modes of objects under the action of fluid force: fluttering, galloping, vortex-induced vibration, and buffeting (Wang et al., 2020a, 2020b; Orrego et al., 2017; Akaydln et al., 2010). Buffeting and vortex-induced vibration are amplitude-limiting vibrations that occur only in a small range of wind speed and remain stationary at most wind speed. Thus, there is no doubt that using these vibrations to harvest energy results in energy wasted. Conversely, as the wind speed increases, the amplitude of galloping and fluttering increases, allowing maximum use of energy. However, since fluttering is a kind of multi-degree-of-freedom vibration, long-term work can easily cause material wear and even damage, so galloping is a better choice. Galloping is an unstable phenomenon that occurs under the action of aerodynamic force. When the wind speed exceeds the cut-in wind speed, its amplitude will increase continuously with the increase of wind speed. Galloping usually occurs in non-streamlined structures such as squares, rectangles, and triangles. It can be regarded as a single-degree-of-freedom self-excited vibration whose oscillation direction is perpendicular to incoming flow, and the overall galloping system can be expressed as (Sun et al., 2019):

$$m\ddot{Y} + \zeta\dot{Y} + kY = \frac{1}{2}\rho V^2 D C_y \qquad \text{(Equation 2.1)}$$

$$C_y(\alpha) = \sum_{i=1}^{n} A_i \left(\frac{\dot{Y}}{V}\right)^i \qquad \text{(Equation 2.2)}$$

$$U_o = \frac{4\zeta m}{\rho D^2 A_1} \qquad \text{(Equation 2.3)}$$

where m is the mass per unit length of the prism, ζ and k are the damping ratio and stiffness of the system, respectively, V and ρ are the wind speed and density, respectively, C_y is the transverse force coefficient, α is attack angle, D is the characteristic length (perpendicular to the incoming flow), Y is the prism displacement, U_o is cut-in wind speed, and A_i is the coefficient of Equation 2.2.

It can be seen from Equation 2.3 that the cut-in wind speed increases with increasing damping. Through our experiments, it is found that the FEP dielectric layer should not be in contact with the Cu electrode in the initial stationary stage, otherwise it will greatly increase the cut-in wind speed of TENG. In order to realize the periodic charging of the FEP dielectric layer without increasing the cut-in wind speed, the rabbit fur brushes are designed on the outside of the Cu electrode on both sides, as shown in Figure 1C. When the vibration amplitude exceeds a certain critical value, the FEP is able to contact with the rabbit fur brushes, as shown in Figure 1E. These soft-contact dielectric brushes can charge the FEP regularly while avoiding a significant increase in cut-in wind speed due to additional damping caused by the contact (Han et al., 2022). And this FEP does not interfere with the motion of the prism when it is in contact with the rabbit fur brushes, because the rabbit fur brushes are very soft. Therefore, the HG P-TENG can effectively utilize galloping for energy harvesting.

Output performance of G-TENG and G-PENG

It can be clearly seen from Figure 2A that the open-circuit voltage (V_{oc}) is basically not generated at lower wind speed, because when the wind speed is lower, the whole system cannot overcome the damping and no galloping phenomenon occurs. When the wind speed exceeds 1.80 m/s, the V_{oc} will increase in steps, which indicates that it starts to gallop. As the wind speed continues to increase, it can be observed that the voltage increases significantly at the initial stage. But when the wind speed reaches 2.95 m/s, as the wind speed continues to increase, the voltage increases only slightly. Although theoretically the voltage of TENG is only related to the contact area and the surface charge density, but not to the speed. However, it is observed in this paper that there is a very slight increase in the V_{oc} with the

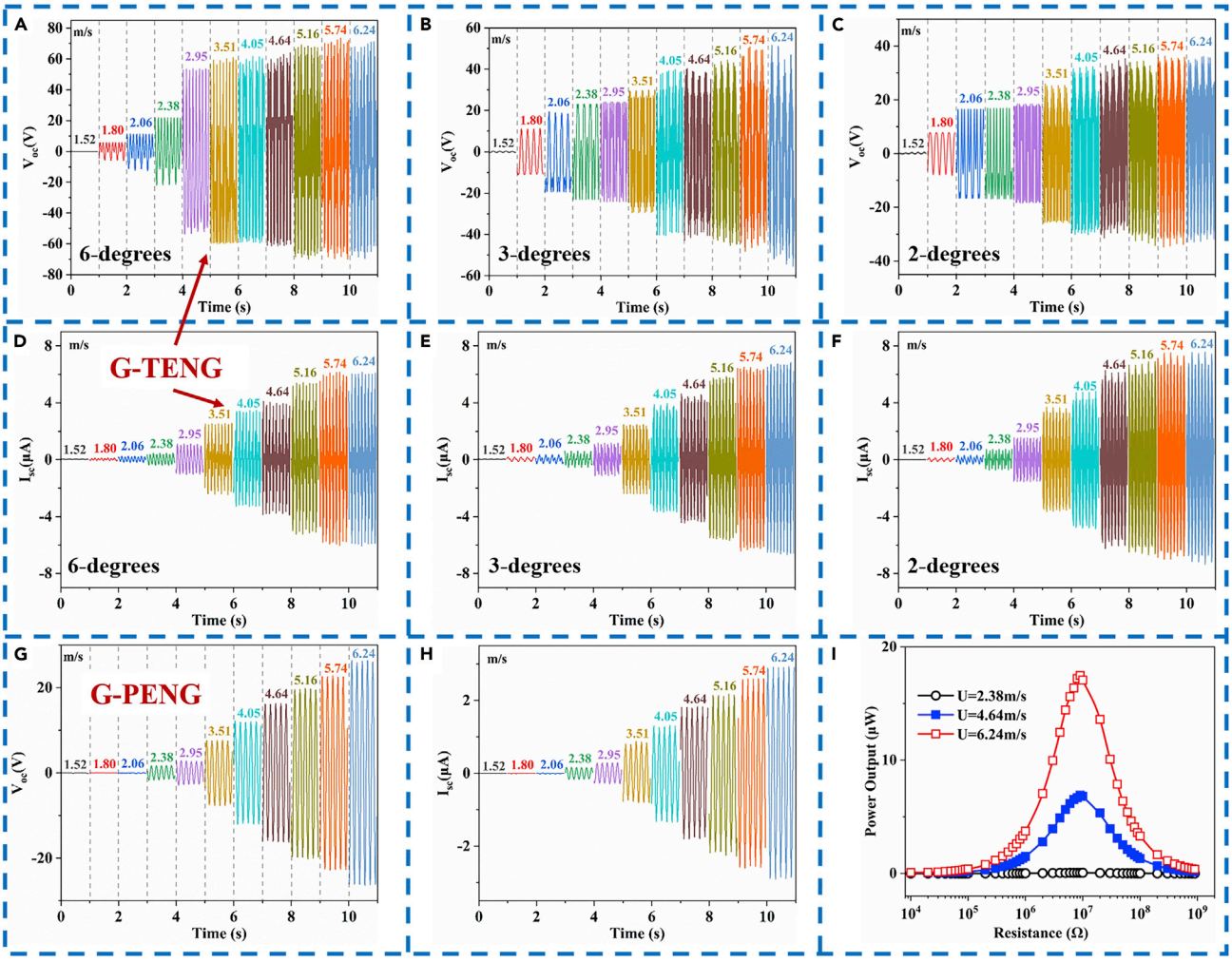

Figure 2. Characteristics of the circuit of 6-degrees, 3-degrees, and 2-degrees HG P-TENG at different wind speeds

(A–F) (A–C) Open-circuit voltage (V_{oc}), (D–F) Short-circuit current (I_{sc}) of 6-degrees, 3-degrees, and 2-degrees G-TENG.

(G–I) (G and H) Open-circuit voltage (V_{oc}) and short-circuit current (I_{sc}) of G-PENG at different wind speeds (I) Variation of G-PENG RMS output power with resistance.

increase of the wind speed, and this increase is due to the increasing amplitude of oscillation with increasing wind speed. Therefore, the FEP dielectric layer is able to sweep a larger area on the bottom Cu electrode, which provides the opportunity to induce more charges, and thus the voltage increases slightly. It can also be observed from Figure S3 that the transfer charge (Q_{sc}) has the same trend as the V_{oc}, and the increase in voltage and charge is due to FEP sweeping more area and thus inducing more charge. As shown by the short-circuit current (I_{sc}) in Figure 2D, it can be clearly seen that the I_{sc} basically increases with the wind speed. The short-circuit current (I_{sc}) can be expressed as:

$$I_{sc} = \frac{dQ_{sc}}{dt} \qquad \text{(Equation 2.4)}$$

There is only a small increase in the transfer charge Q_{sc} as the wind speed increases, and the vibration frequency of the system changes very little (Shi et al., 2020). This means that the time required for one cycle of prism motion is essentially constant, but the amplitude increases with the wind speed. For the cantilever beam, when the prism moves toward the middle of the two Cu electrodes, the speed is the largest, and when it moves to the two sides, the speed decreases until zero, as shown in Figure S4. And with the increase of the amplitude, the speed of the prism across the two Cu electrodes increases continuously and the crossing time decreases, so the I_{sc} will will keep increasing.

According to the principle of TENG, the electron transfer phenomenon occurs only when the FEP dielectric layer moves between two Cu electrodes, so we further segment the 6-degrees electrodes into 3-degrees and 2-degrees which can increase the frequency of charge transfer and the results are shown in Figure S5. Comparing Figures 2A–2C, 6-degrees G-TENG has the peak voltage and current of about 140 V and 12.5 μA when the wind speed is 6.24 m/s. With increasing the number of electrodes, the open-circuit voltage gradually decreases while the output current increases (Pang et al., 2021). For the 2-degrees G-TENG, the peak voltage and current is about 74 V and 16.7 μA which have a 34% improvement rather than 6-degrees. Also, more current cycles are observed in one cycle for finer electrodes; the number of current peaks for 6-degrees, 3-degrees, and 2-degrees is 6, 12, and 20, respectively, as shown in Figure S6. In addition, the transfer charge also decreases with the increasing number of electrodes, which is mainly due to the decrease in the number of triboelectric charge (Lu et al., 2021). Since the same piezoelectric sheet was used throughout the experiment, only the piezoelectric performance of the 6-degrees G-TENG is shown in the paper. The 3-degrees G-TENG and 2-degrees G-TENG have basically the same piezoelectric properties. Figures 2G and 2H give the voltage and current of the piezoelectric nanogenerator at various wind speeds, and the corresponding optimum resistance is $9 \times 10^6 \Omega$ as shown in Figure 2I, and the current between 1s is shown in Figure S7. The output power of the piezoelectric nanogenerator is basically the same in these three cases. All of them increase with the wind speed, and the maximum output peak voltage and current is 52.8 V and 5.86 μA when the wind speed is 6.24 m/s. In addition to this, it is observed that the RMS current varies essentially linearly with the wind speed (Figure S8), which implies the ability to work as a wind speed sensor (Ye et al., 2021). Figure S9 shows voltage variation of PENG with attack angle (Here the attack angle refers to the angle between the incoming wind and the cantilever beam at stationary). When the attack angle is less than 12°, the voltage of PENG basically does not change, which also indicates that the galloping is basically not influenced by the change of attack angle. As the attack angle continues to increase, the amplitude will gradually decrease until it reduced to zero. Therefore, when the attack angle is less than $\pm 12°$, the HG-PENG is still able to harvest energy normally. And in future research, we will further explore the use of a circular array approach to harvest 360° of wind energy. Therefore, it is feasible that this triboelectric-piezoelectric hybrid nanogenerator can effectively utilize PENG and TENG for energy harvesting.

Application of HG P-TENG

To demonstrate the practical application capability of the HG P-TENG, this combined G-PENG and G-TENG hybrid nanogenerator device and capacitor connected through a full-bridge rectifier are able to drive a thermohygrometer, as shown in Figure 4H and Vedio S2. It is also capable of driving more than about 100 green LEDs to glow brightly, as shown in Figure 4G. And the circuit diagrams of HG P-TENG in lighting and charging capacitors are shown in Figure S10. Figure 3 shows the voltage curves of HG P-TENG charged to 10 V at a wind speed of 6.24 m/s for capacitors with capacities of 10, 22, and 47 μF. In the cases of 3 different capacitances, the charging rate of the 2-degrees G-TENG is much higher than that of the 6-degrees G-TENG. For a 47 μF capacitor, it takes only 122 s for the 2-degrees, 137 s for the 3-degrees, and 182 s for the 6-degrees, while the charging time of PENG is 314 s. This shows that no matter which TENG is, its charging efficiency is much higher than that of PENG. The charging time of 2-degrees G-TENG is reduced by 33% compared with that of 6-degrees G-TENG, which greatly improves the performance of G-TENG. Furthermore, the charging time of the HG P-TENG (2-degrees) is only 88 s, which is reduced by 52% compared with 6-degrees G-TENG. The saturation voltages of different capacitors are shown in Figure S11, and we will conduct more detailed charging studies in future experiments. Moreover, a comparison with other energy harvesters is described in Table S2 which indicates that HG P-TENG has a higher charging efficiency.

Figures 4A–4C plot the RMS power of these three types G-TENG at different resistances. As shown in Figure 4A, it can be seen that its maximum power increases with the increase of wind speed. Although the output power decreases after segmenting the electrodes, it is able to transfer more charge in a single cycle. Moreover, it is also observed that the optimal resistance decreases with increasing wind speed. Figure 4D illustrates the variation of the RMS power of G-TENG and G-PENG with resistance with three different degrees when the wind speed is 6.24 m/s. It can also be found that the finer the electrodes, the smaller the optimal resistance will be, mainly because finer electrodes will have higher capacitance. Further to understand its output power variation, Figure 4E also depicts the RMS power with wind speed for three types of G-TENG and G-PENG. According to $P = V_{rms}/R$, the amount of the resistance needs to be known when calculating the RMS power; however, the optimal resistance of the G-TENG is changing as the wind speed

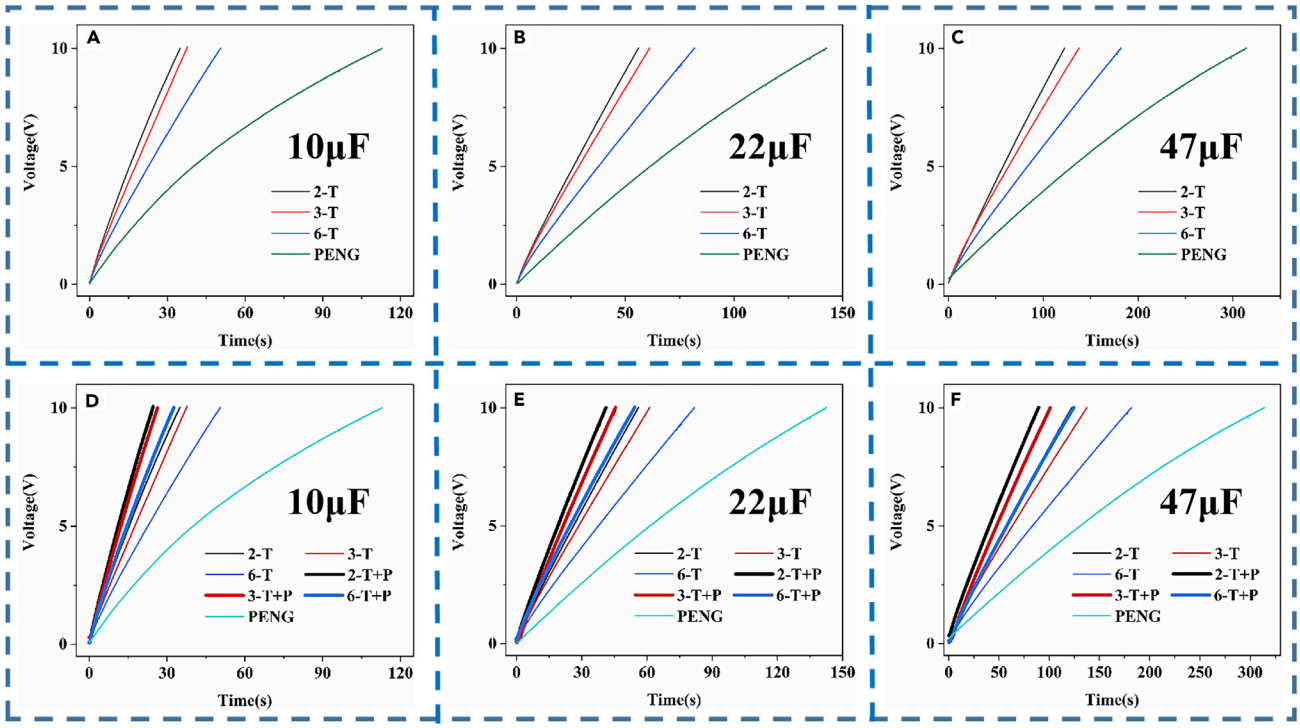

Figure 3. Performance of HG P-TENG for charging different capacitors

(A–C) 10μF, (b)22μF, and (c)47μF capacitors charging curves of 6-degrees, 3-degrees, 2-degrees G-TENG and G-PENG.

(D–F) 10μF, (e)22μF, and (f)47μF capacitors charging curves of HG P-TENG. (2-T indicates 2-degrees G-TENG and 2-T + P indicates 2-degrees G-TENG and G-PENG).

is constantly varying. Therefore, the optimal resistance at 6.24 m/s wind speed is adopted. For 6-degrees, 3-degrees, and 2-degrees G-TENG, the optimal resistance will use 1×10^7, 4×10^6, and $3 \times 10^6\Omega$, respectively. With the increasing of wind speed, the power of both G-TENG and G-PENG is increasing, the power of G-PENG is still increasing until 6.24 m/s. However, when the wind speed increases to 5.74 m/s, the power of G-TENG will not increase and will even decrease slightly. This is because when the wind speed starts to increase from a low speed, its tribo-surface area will also keep increasing. When the wind speed reaches a critical value, the tribo-surface area has reached the maximum value, and its output voltage remains basically constant, as shown in Figure S12, hence its power will not continue to increase. When the wind speed is 6.24 m/s, the RMS power of 6-degrees, 3-degrees, and 2-degrees G-TENG is 52.2, 38.5, and 34.7 μW, respectively, while the power of G-PENG is 16.7 μW. The overall RMS power of HG P-TENG is 68.9 μW which its RMS power density is about 22.7 mW/m^2. The peak power of these three structures is presented in Figure S13. And the peak power and power density of HG P-TENG is 1.27 mW and 0.4 W/m^2. Moreover, G-TENG has lower cut-in wind speed, as can be seen from Figure 2B; when the wind speed is 1.80 m/s, the voltage of 6-degrees G-TENG is about 15 V, while PENG is basically 0 V.

The results of the durability test are shown in Figure 4F, using 6-degrees G-TENG for the test. It can be observed that after about 250,000 cycles, there is only a slight decrease in output voltage, which demonstrates the excellent durability of the HG P-TENG. And Figure S14 displays the scanning electron microscope images of the FEP material before and after the 250,000 test cycles. The images indicate only a few tiny scratches on the surface of the FEP, and no significant damage occurred. The major reason is that HG P-TENG adopts non-contact electrostatic induction and soft contact with rabbit fur, which greatly reduces the wear on the material, and the rabbit fur can also effectively supplement the charge for the FEP.

For long-distance pipeline systems, many sensors are required to monitor parameters such as temperature and pressure of the gas in the pipeline. For this distributed energy supply, traditional batteries and wire methods undoubtedly have many drawbacks, so this hybrid nanogenerator will have great advantages in long-distance intelligent pipeline monitoring. On the one hand, the HG P-TENG can be installed in pipeline

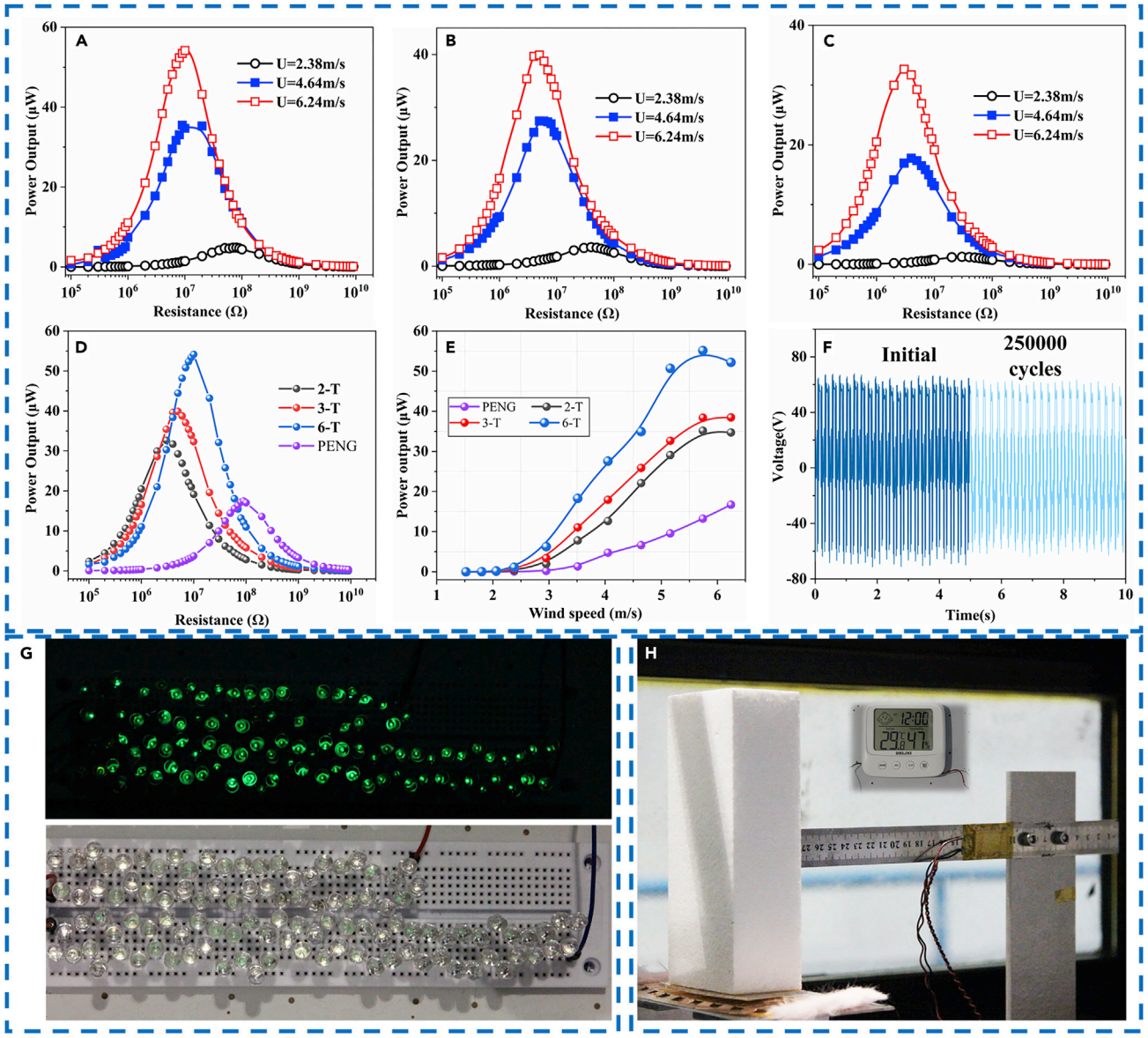

Figure 4. Output Performance of the HG P-TENG

(A–E) Top panel: RMS power resistance profile of (A) 6-degrees, (B) 3-degrees, and (C) 2-degrees G-TENG at various wind speeds. Middle panel: (D) Comparison of RMS power with resistance for 6-degrees, 3-degrees, 2-degrees G-TENG, and G-PENG at wind speed of 6.24 m/s (E) 6-degrees, 3-degrees, 2-degrees G-TENG, and G-PENG RMS power variation with wind speed.

(F) Durability of the G-TENG device for about 250,000 cycles at 6.24 m/s.

(G) Photograph of the HG P-TENG lighting up more than 100 LEDs.

(I) Photograph of the HG P-TENG as a power source to drive a thermohygrometer.

to effectively drive the sensors to monitor the temperature, humidity, pressure, etc. of the gas in pipeline. On the other hand, it can drive the signal transmission elements and actuators to feedback abnormal signals and eliminate problems in time to ensure the safe operation of pipeline system. The use of HG P-TENG provides an effective solution for the long-distance intelligent pipeline monitoring systems.

Conclusions

In the paper, a galloping-based triboelectric-piezoelectric hybrid nanogenerator (HG P-TENG) is proposed to harvest gas energy in long-distance pipeline, which can provide continuous energy supply for alarm devices and sensors. The use of galloping for energy harvesting effectively reduces material wear and

improves the reliability of GTENG. And through the rational construction design of HG P-TENG, the cut-in wind speed and the wear of TENG material are effectively reduced, thus improving the efficiency and durability of the device. Moreover, with periodic contact, FEP can be recharged, offering the possibility of long-term, efficient energy harvesting. Furthermore, by segmenting the electrodes, the energy harvesting efficiency is greatly improved. The maximum I_{sc} of 2-degrees G-TENG has a 34% improvement rather than 6-degrees. Comparing the capacitor charging time, the charging time of 2-degrees G-TENG and HG P-TENG (2-degrees) is reduced by 33% and 52% compared with that of 6-degrees G-TENG, respectively. Then, at a wind speed of 6.24 m/s, the maximum RMS output power of the 6-degrees, 3-degrees, 2-degrees G-TENG, and G-PENG is 52.2, 38.5, 34.7, and 16.7 μW, respectively. In addition, the feasibility of this HG P-TENG to power a thermohygrometer is also demonstrated. This study uses a piezoelectric-triboelectric hybrid nanogenerator to harvest energy from airflow in pipes, which has great potential in long-distance smart pipeline monitoring systems.

Limitations of the study

Although, HG P-TENG has a high energy harvesting efficiency when the direction of incoming flow is determined. Due to the characteristics of the vibration form of galloping, it can only be used to harvest wind energy within a certain angle of attack, and when this angle of attack is exceeded, larger winds can even cause damage to the HG P-TENG. So, a structure that automatically rotates according to the wind direction is to be considered in future solutions.

STAR★METHODS

Detailed methods are provided in the online version of this paper and include the following:

- KEY RESOURCES TABLE
- RESOURCE AVAILABILITY
  - Lead contact
  - Materials availability
  - Data and code availability
- EXPERIMENTAL MODEL AND SUBJECT DETAILS
- METHOD DETAILS
  - Fabrication of the hybrid nanogenerator
  - Electrical output signal measurement
- QUANTIFICATION AND STATISTICAL ANALYSIS
- ADDITIONAL RESOURCES

SUPPLEMENTAL INFORMATION

Supplemental information can be found online at https://doi.org/10.1016/j.isci.2022.105374.

ACKNOWLEDGMENTS

This research is supported by the National Key R&D Program of China (No. 2018FYA0305800) and the National Natural Science Foundation of China (No. 11872362).

AUTHOR CONTRIBUTIONS

Conceptualization: W.W. and Z.Y.; Methodology: W.W. and Z.Y.; Software: W.W.; Investigation: W.W.; Writing original draft: W.W.; Formal analysis: W.W.; Validation: W.W.; Writing - review & editing: W.T. and Z.Y.; Supervision: W.T. and Z.Y.; Funding Acquisition: Z.Y.

DECLARATION OF INTERESTS

The authors declare no competing interests.

Received: June 13, 2022
Revised: September 7, 2022
Accepted: October 13, 2022
Published: November 18, 2022

SUPPORTING CITATIONS

The following references appear in the Supplemental Information: Huang et al., 2021; Tashiro et al., 2002; Wu et al., 2014; Zhang et al., 2020b.

REFERENCES

Abdelkefi, A., Hasanyan, A., Montgomery, J., Hall, D., and Hajj, M.R. (2014). Incident flow effects on the performance of piezoelectric energy harvesters from galloping vibrations. Theor. Appl. Mech. Lett. *4*, 022002. https://doi.org/10.1063/2.1402202.

Akaydln, H.D., Elvin, N., and Andreopoulos, Y. (2010). Wake of a cylinder: a paradigm for energy harvesting with piezoelectric materials. Exp. Fluids *49*, 291–304. https://doi.org/10.1007/s00348-010-0871-7.

Alhadidi, A.H., Alhussein, H., and Daqaq, M.F. (2020). Improving the sensitivity of galloping energy harvesters to flow fluctuations. Appl. Phys. Lett. *116*, 2–7. https://doi.org/10.1063/5.0011118.

Avila Bernal, A.G., and Linares García, L.E. (2012). The modelling of an electromagnetic energy harvesting architecture. Appl. Math. Model. *36*, 4728–4741. https://doi.org/10.1016/j.apm.2011.12.007.

Bae, J., Lee, J., Kim, S., Ha, J., Lee, B.S., Park, Y., Choong, C., Kim, J.B., Wang, Z.L., Kim, H.Y., et al. (2014). Flutter-driven triboelectrification for harvesting wind energy. Nat. Commun. *5*, 1–9. https://doi.org/10.1038/ncomms5929.

Basset, P., Galayko, D., Cottone, F., Guillemet, R., Blokhina, E., Marty, F., and Bourouina, T. (2014). Electrostatic vibration energy harvester with combined effect of electrical nonlinearities and mechanical impact. J. Micromech. Microeng. *24*. https://doi.org/10.1088/0960-1317/24/3/035001.

Beeby, S.P., Tudor, M.J., and White, N.M. (2006). Energy harvesting vibration sources for microsystems applications. Meas. Sci. Technol. *17*. https://doi.org/10.1088/0957-0233/17/12/R01.

Chen, B., Yang, Y., and Wang, Z.L. (2018). Scavenging wind energy by triboelectric nanogenerators. Adv. Energy Mater. *8*, 1–13. https://doi.org/10.1002/aenm.201702649.

Chen, P., An, J., Shu, S., Cheng, R., Nie, J., Jiang, T., and Wang, Z.L. (2021). Super-durable, low-wear, and high-performance Fur-brush triboelectric nanogenerator for wind and water energy harvesting for smart agriculture. Adv. Energy Mater. *11*, 1–10. https://doi.org/10.1002/aenm.202003066.

Davies, D.K. (1969). Charge generation on dielectric surfaces. J. Phys. D Appl. Phys. *2*, 1533–1537. https://doi.org/10.1088/0022-3727/2/11/307.

Fan, F.R., Tian, Z.Q., and Lin Wang, Z. (2012). Flexible triboelectric generator. Nano. Energy *1*, 328–334. https://doi.org/10.1016/j.nanoen.2012.01.004.

Fu, X., Xu, S., Gao, Y., Zhang, X., Liu, G., Zhou, H., Lv, Y., Zhang, C., and Wang, Z.L. (2021). Breeze-wind-energy-powered autonomous wireless anemometer based on rolling contact-electrification. ACS Energy Lett. *6*, 2343–2350. https://doi.org/10.1021/acsenergylett.1c00704.

Han, J., Feng, Y., Chen, P., Liang, X., Pang, H., Jiang, T., and Wang, Z.L. (2022). Wind-Driven soft-contact rotary triboelectric nanogenerator based on rabbit Fur with high performance and durability for smart farming. Adv. Funct. Mater. *32*, 1–8. https://doi.org/10.1002/adfm.202108580.

He, J., Fan, X., Zhao, D., Cui, M., Han, B., Hou, X., and Chou, X. (2022a). A high-efficient triboelectric-electromagnetic hybrid nanogenerator for vibration energy harvesting and wireless monitoring. Sci. China Inf. Sci. *65*, 1–9. https://doi.org/10.1007/s11432-020-3081-4.

He, J., Li, S., Hou, X., Zhou, Y., Li, H., Cui, M., Guo, T., Wang, X., Mu, J., Geng, W., and Chou, X. (2022b). A non-contact flexible pyroelectric sensor for wireless physiological monitoring system. Sci. China Inf. Sci. *65*, 1–11. https://doi.org/10.1007/s11432-020-3175-6.

Hu, G., Tse, K.T., Wei, M., Naseer, R., Abdelkefi, A., and Kwok, K.C.S. (2018a). Experimental investigation on the efficiency of circular cylinder-based wind energy harvester with different rod-shaped attachments. Appl. Energy *226*, 682–689. https://doi.org/10.1016/j.apenergy.2018.06.056.

Hu, J., Pu, X., Yang, H., Zeng, Q., Tang, Q., Zhang, D., Hu, C., and Xi, Y. (2019). A flutter-effect-based triboelectric nanogenerator for breeze energy collection from arbitrary directions and self-powered wind speed sensor. Nano Res. *12*, 3018–3023. https://doi.org/10.1007/s12274-019-2545-y.

Hu, Y., Yang, B., Chen, X., Wang, X., and Liu, J. (2018b). Modeling and experimental study of a piezoelectric energy harvester from vortex shedding-induced vibration. Energy Convers. Manag. *162*, 145–158. https://doi.org/10.1016/j.enconman.2018.02.026.

Huang, X., Qin, Q., Wang, X., Xiang, H., Zheng, J., Lu, Y., Lv, C., Wu, K., Yan, L., Wang, N., et al. (2021). Piezoelectric nanogenerator for highly sensitive and synchronous multi-stimuli sensing. ACS Nano *15*, 19783–19792. https://doi.org/10.1021/acsnano.1c07236.

Jiang, D., Liu, G., Li, W., Bu, T., Wang, Y., Zhang, Z., Pang, Y., Xu, S., Yang, H., and Zhang, C. (2020). A leaf-shaped triboelectric nanogenerator for multiple ambient mechanical energy harvesting. IEEE Trans. Power Electron. *35*, 25–32. https://doi.org/10.1109/TPEL.2019.2921152.

Li, C., Liu, D., Xu, C., Wang, Z., Shu, S., Sun, Z., Tang, W., and Wang, Z.L. (2021). Sensing of joint and spinal bending or stretching via a retractable and wearable badge reel. Nat. Commun. *12*, 1–11. https://doi.org/10.1038/s41467-021-23207-8.

Li, X., Cao, Y., Yu, X., Xu, Y., Yang, Y., Liu, S., Cheng, T., and Wang, Z.L. (2022). Breeze-driven triboelectric nanogenerator for wind energy harvesting and application in smart agriculture. Appl. Energy *306*, 117977. https://doi.org/10.1016/j.apenergy.2021.117977.

Li, X., Yin, X., Zhao, Z., Zhou, L., Liu, D., Zhang, C., Zhang, C., Zhang, W., Li, S., Wang, J., and Wang, Z.L. (2020). Long-lifetime triboelectric nanogenerator operated in conjunction modes and low crest factor. Adv. Energy Mater. *10*, 1–8. https://doi.org/10.1002/aenm.201903024.

Lin, H., He, M., Jing, Q., Yang, W., Wang, S., Liu, Y., Zhang, Y., Li, J., Li, N., Ma, Y., et al. (2019). Angle-shaped triboelectric nanogenerator for harvesting environmental wind energy. Nano Energy *56*, 269–276. https://doi.org/10.1016/jnanoen.2018.11.037.

Liu, S., Li, X., Wang, Y., Yang, Y., Meng, L., Cheng, T., and Wang, Z.L. (2021). Magnetic switch structured triboelectric nanogenerator for continuous and regular harvesting of wind energy. Nano Energy *83*, 105851. https://doi.org/10.1016/j.nanoen.2021.105851.

Lu, P., Pang, H., Ren, J., Feng, Y., An, J., Liang, X., Jiang, T., and Wang, Z.L. (2021). Swing-structured triboelectric–electromagnetic hybridized nanogenerator for breeze wind energy harvesting. Adv. Mater. Technol. *6*, 1–10. https://doi.org/10.1002/admt 202100496.

McCarty, L.S., and Whitesides, G.M. (2008). Electrostatic charging due to separation of ions at interfaces: contact electrification of ionic electrets. Angew. Chemie Int. Ed. *47*, 2188–2207. https://doi.org/10.1002/anie.200701812.

Mitcheson, P.D., Miao, P., Stark, B.H., Yeatman, E.M., Holmes, A.S., and Green, T.C. (2004). MEMS electrostatic micropower generator for low frequency operation. Sensors Actuat. A Phys. *115*, 523–529. https://doi.org/10.1016/j.sna.2004.04.026.

Olsen, M., Zhang, R., Örtegren, J., Andersson, H., Yang, Y., and Olin, H. (2019). Frequency and voltage response of a wind-driven fluttering triboelectric nanogenerator. Sci. Rep. *9*, 1–6. https://doi.org/10.1038/s41598-019-42128-7.

Orrego, S., Shoele, K., Ruas, A., Doran, K., Caggiano, B., Mittal, R., and Kang, S.H. (2017). Harvesting ambient wind energy with an inverted piezoelectric flag. Appl. Energy *194*, 212–222. https://doi.org/10.1016/j.apenergy.2017.03.016.

Pang, H., Feng, Y., An, J., Chen, P., Han, J., Jiang, T., and Wang, Z.L. (2021). Segmented swing-structured Fur-based triboelectric nanogenerator for harvesting blue energy toward marine environmental applications. Adv. Funct. Mater. *31*, 1–10. https://doi.org/10.1002/adfm.202106398.

Park, J., Han, M., Kim, G., Jung, Y., and Cho, H. (2019). Tree-wrapped triboelectric generator for harvesting wind energy. J. Nanosci. Nanotechnol. *20*, 239–244. https://doi.org/10.1166/jnn.2020.17281.

Ren, Z., Wang, Z., Liu, Z., Wang, L., Guo, H., Li, L., Li, S., Chen, X., Tang, W., and Wang, Z.L. (2020). Energy harvesting from breeze wind (0.7–6 m/s^{-1}) using ultra-stretchable triboelectric nanogenerator. Adv. Energy Mater. *10*, 1–9. https://doi.org/10.1002/aenm.202001770.

Ren, Z., Wang, Z., Wang, F., Li, S., and Wang, Z.L. (2021). Vibration behavior and excitation mechanism of ultra-stretchable triboelectric nanogenerator for wind energy harvesting. Extrem. Mech. Lett. *45*, 101285. https://doi.org/10.1016/j.eml.2021.101285.

Shi, M., Holmes, A.S., and Yeatman, E.M. (2020). Piezoelectric wind velocity sensor based on the variation of galloping frequency with drag force. Appl. Phys. Lett. *116*. https://doi.org/10.1063/5.0012244.

Sun, W., Jo, S., and Seok, J. (2019). Development of the optimal bluff body for wind energy harvesting using the synergetic effect of coupled vortex induced vibration and galloping phenomena. Int. J. Mech. Sci. *156*, 435–445. https://doi.org/10.1016/j.ijmecsci.201904.019.

Tashiro, R., Kabei, N., Katayama, K., Tsuboi, F., and Tsuchiya, K. (2002). Development of an electrostatic generator for a cardiac pacemaker that harnesses the ventricular wall motion. J. Artif. Organs *5*, 239–245. https://doi.org/10.1007/s100470200045.

Tee, B.C.K., Wang, C., Allen, R., and Bao, Z. (2012). An electrically and mechanically self-healing composite with pressure- and flexion-sensitive properties for electronic skin applications. Nat. Nanotechnol. *7*, 825–832. https://doi.org/10.1038/nnano.2012.192.

Vicente-Ludlam, D., Barrero-Gil, A., and Velazquez, A. (2014). Optimal electromagnetic energy extraction from transverse galloping. J. Fluids Struct. *51*, 281–291. https://doi.org/10.1016/j.jfluidstructs.2014.09.007.

Wang, Z.L. (2014). Triboelectric nanogenerators as new energy technology and self-powered sensors - principles, problems and perspectives. Faraday Discuss. *176*, 447–458. https://doi.org/10.1039/c4fd00159a.

Wang, C., Hwang, D., Yu, Z., Takei, K., Park, J., Chen, T., Ma, B., and Javey, A. (2013). User-interactive electronic skin for instantaneous pressure visualization. Nat. Mater. *12*, 899–904. https://doi.org/10.1038/nmat3711.

Wang, J., Su, Z., Li, H., Ding, L., Zhu, H., and Gaidai, O. (2020a). Imposing a wake effect to improve clean marine energy harvesting by flow-induced vibrations. Ocean Eng. *208*, 107455. https://doi.org/10.1016/j.oceaneng.2020.107455.

Wang, J., Zhang, C., Gu, S., Yang, K., Li, H., Lai, Y., and Yurchenko, D. (2020b). Enhancement of low-speed piezoelectric wind energy harvesting by bluff body shapes: spindle-like and butterfly-like cross-sections. Aerosp. Sci. Technol. *103*, 105898. https://doi.org/10.1016/j.ast.2020.105898.

Wang, Q., Zou, H.X., Zhao, L.C., Li, M., Wei, K.X., Huang, L.P., and Zhang, W.M. (2020c). A synergetic hybrid mechanism of piezoelectric and triboelectric for galloping wind energy harvesting. Appl. Phys. Lett. *117*. https://doi.org/10.1063/5.0014484.

Wang, Y., Wang, J., Xiao, X., Wang, S., Kien, P.T., Dong, J., Mi, J., Pan, X., Wang, H., and Xu, M. (2020d). Multi-functional wind barrier based on triboelectric nanogenerator for power generation, self-powered wind speed sensing and highly efficient windshield. Nano Energy *73*, 104736. https://doi.org/10.1016/j.nanoen.2020.104736.

Wang, W., Huang, J., and Yao, Z. (2021). Cut-corner prism piezoelectric energy harvester based on galloping enhancement mechanism. Energy Rep. *7*, 6366–6374. https://doi.org/10.1016/j.egyr.2021.09.081.

Wang, X., Niu, S., Yin, Y., Yi, F., You, Z., and Wang, Z.L. (2015). Triboelectric nanogenerator based on fully enclosed rolling spherical structure for harvesting low-frequency water wave energy. Adv. Energy Mater. *5*, 1–9. https://doi.org/10.1002/aenm.201501467.

Wang, X., Yin, Y., Yi, F., Dai, K., Niu, S., Han, Y., Zhang, Y., and You, Z. (2017). Bioinspired stretchable triboelectric nanogenerator as energy-harvesting skin for self-powered electronics. Nano Energy *39*, 429–436. https://doi.org/10.1016/j.nanoen.2017.07.022.

Wang, Y., Liu, X., Chen, T., Wang, H., Zhu, C., Yu, H., Song, L., Pan, X., Mi, J., Lee, C., and Xu, M. (2021). An underwater flag-like triboelectric nanogenerator for harvesting ocean current energy under extremely low velocity condition. Nano Energy *90*, 106503. https://doi.org/10.1016/j.nanoen.2021.106503.

Wen, Z., Chen, J., Yeh, M.H., Guo, H., Li, Z., Fan, X., Zhang, T., Zhu, L., and Wang, Z.L. (2015). Blow-driven triboelectric nanogenerator as an active alcohol breath analyzer. Nano Energy *16*, 38–46. https://doi.org/10.1016/j.nanoen.2015.06.006.

Wu, Y., Zhong, X., Wang, X., Yang, Y., and Wang, Z.L. (2014). Hybrid energy cell for simultaneously harvesting wind, solar, and chemical energies. Nano Res. *7*, 1631–1639. https://doi.org/10.1007/s12274-014-0523-y.

Xia, Y., Tian, Y., Zhang, L., Ma, Z., Dai, H., Meng, B., and Peng, Z. (2021). An optimized flutter-driven triboelectric nanogenerator with a low cut-in wind speed. Micromachines *12*, 1–9. https://doi.org/10.3390/mi12040366.

Xie, Y., Wang, S., Lin, L., Jing, Q., Lin, Z.H., Niu, S., Wu, Z., and Wang, Z.L. (2013). Rotary triboelectric nanogenerator based on a hybridized mechanism for harvesting wind energy. ACS Nano *7*, 7119–7125. https://doi.org/10.1021/nn402477h.

Xu, F., Dong, S., Liu, G., Pan, C., Guo, Z.H., Guo, W., Li, L., Liu, Y., Zhang, C., Pu, X., and Wang, Z.L. (2021). Scalable fabrication of stretchable and washable textile triboelectric nanogenerators as constant power sources for wearable electronics. Nano Energy *88*, 106247. https://doi.org/10.1016/j.nanoen.2021.106247.

Yang, D., Ni, Y., Kong, X., Li, S., Chen, X., Zhang, L., and Wang, Z.L. (2021). Self-Healing and elastic triboelectric nanogenerators for muscle motion monitoring and photothermal treatment. ACS Nano *15*, 14653–14661. https://doi.org/10.1021/acsnano.1c04384.

Ye, C., Dong, K., An, J., Yi, J., Peng, X., Ning, C., and Wang, Z.L. (2021). A triboelectric-electromagnetic hybrid nanogenerator with broadband working range for wind energy harvesting and a self-powered wind speed sensor. ACS Energy Lett. *6*, 1443–1452. https://doi.org/10.1021/acsenergylett.1c00244.

Zeng, Q., Wu, Y., Tang, Q., Liu, W., Wu, J., Zhang, Y., Yin, G., Yang, H., Yuan, S., Tan, D., et al. (2020). A high-efficient breeze energy harvester utilizing a full-packaged triboelectric nanogenerator based on flow-induced vibration. Nano Energy *70*, 104524. https://doi.org/10.1016/j.nanoen.2020.104524.

Zhang, C., Liu, Y., Zhang, B., Yang, O., Yuan, W., He, L., Wei, X., Wang, J., and Wang, Z.L. (2021a). Harvesting wind energy by a triboelectric nanogenerator for an intelligent high-speed train system. ACS Energy Lett. *6*, 1490–1499. https://doi.org/10.1021/acsenergylett.1c00368.

Zhang, C., Zhou, L., Cheng, P., Liu, D., Zhang, C., Li, X., Li, S., Wang, J., and Wang, Z.L. (2021b). Bifilar-pendulum-assisted multilayer-structured triboelectric nanogenerators for wave energy harvesting. Adv. Energy Mater. *11*, 1–10. https://doi.org/10.1002/aenm.202003616.

Zhang, L., Meng, B., Xia, Y., Deng, Z., Dai, H., Hagedorn, P., Peng, Z., and Wang, L. (2020a). Galloping triboelectric nanogenerator for energy harvesting under low wind speed. Nano Energy *70*, 104477. https://doi.org/10.1016/j.nanoen.2020.104477.

Zhang, Y., Zeng, Q., Wu, Y., Wu, J., Yuan, S., Tan, D., Hu, C., and Wang, X. (2020b). An ultra-durable windmill-like hybrid nanogenerator for steady and efficient harvesting of low-speed wind energy. Nano Micro Lett. https://doi.org/10.1007/s40820-020-00513-2.

Zhu, G., Pan, C., Guo, W., Chen, C.Y., Zhou, Y., Yu, R., and Wang, Z.L. (2012). Triboelectric-generator-driven pulse electrodeposition for micropatterning. Nano Lett. *12*, 4960–4965. https://doi.org/10.1021/nl302560k.

STAR★METHODS

KEY RESOURCES TABLE

REAGENT or RESOURCE	SOURCE	IDENTIFIER
Chemicals, peptides, and recombinant proteins		
Copper Tape	Suzhou dry ding electronic technology co., LTD	QD68-SDT-005
Piezoelectric Sheets	VKINGING ELECTRONICS (SHEN ZHEN)	LDT0-028K
Fluorinated Ethylene Propylene (FEP)	Suzhou Zeyou Fluoroplastic Material Technology Co., Ltd	N/A
Rabbit Fur	Hefei Wanchong Pet Products Co., Ltd	N/A

RESOURCE AVAILABILITY

Lead contact

Further information and requests for resources should be directed to and will be fulfilled by the lead contact, Zhaohui Yao (yaozh@ucas.edu.cn).

Materials availability

This study did not generate new materials. Materials used in the study are commercially available.

Data and code availability

- All data reported in this paper will be shared by the lead contact upon request.
- This paper does not report original code.
- Any additional information required to reanalyze the data reported in this paper is available from the lead contact upon request.

EXPERIMENTAL MODEL AND SUBJECT DETAILS

This study does not use experimental methods typical in the life sciences.

METHOD DETAILS

Fabrication of the hybrid nanogenerator

Two pieces piezoelectric sheets (LDT0-028K) are attached to two sides of the cantilever beam. The piezoelectric sheet is 41 mm long, 16 mm wide. The length, width and height of the cantilever beam are 200 × 26 × 1 mm. The prism made by the electric wire cutting machine is fixed on the top of the cantilever beam with special foam glue, and the prism size is: 190 × 80 × 50 mm. The curved acrylic plate with FEP is adhered to the bottom of the foam prism as a dielectric layer with a thickness of 0.1 mm which Figure S15 has shown that FEP thickness is 0.1 mm is better. And the bottom of the FEP is 4 mm away from the Cu electrode layer. The curved electrode layer is fixed on an acrylic plate by double-sided tape, and is made of copper tape with a thickness of 0.03 mm. The electrode layer is annular, and the width of the electrode layer is 60 mm. For 6-degrees, 3-degreepairs, and 2-degrees of Cu electrodes, the arc angles are 6°, 3 and 2°, respectively, and the spacing between adjacent two electrodes are 0.6°, 0.27 and 0.18°, respectively (Figure S5). This allows us to ensure that the total angle is 39°. The rabbit fur on the outside of the electrode is taped to the acrylic plate at the bottom.

Electrical output signal measurement

The open circuit voltage and short circuit current of the G-TENG are measured by a Keithley 6514 electrometer. A Keysight DSOX1204G oscilloscope is used to measure the voltage of the G-PENG.

QUANTIFICATION AND STATISTICAL ANALYSIS

This study does not include statistical analysis or quantification.

ADDITIONAL RESOURCES

This study has not generated or contributed to a new website/forum.